Article

A human brain network linked to restoration of consciousness after deep brain stimulation

Aaron E. L. Warren [1,2] ✉, Marina Raguž[3,4], Helen Friedrich[2,5], Frederic L. W. V. J. Schaper [2], Jordy Tasserie[2], Samuel B. Snider[2], Jian Li [6,7], Melissa M. J. Chua[1,2], Konstantin Butenko[2], Maximilian U. Friedrich [2], Rohan Jha[1,2], Juan E. Iglesias[6,8,9], Patrick W. Carney[10,11], David Fischer[12], Michael D. Fox [2], Aaron D. Boes [13], Brian L. Edlow [6,7], Andreas Horn [2,7,14,15], Darko Chudy[3,16,17] & John D. Rolston [1,2,17] ✉

Disorders of consciousness are characterized by severe impairments in arousal and awareness. Deep brain stimulation is a potential treatment, but outcomes vary—possibly due to differences in patient characteristics, electrode placement, or the specific brain network engaged. We describe 40 patients with disorders of consciousness undergoing deep brain stimulation targeting the thalamic centromedian-parafascicular complex. Improvements in consciousness are associated with better-preserved gray matter, particularly in the striatum. Electric field modeling reveals that stimulation is most effective when it extends below the centromedian nucleus, engaging the inferior parafascicular nucleus and the adjacent ventral tegmental tract—a pathway that connects the brainstem and hypothalamus and runs along the midbrain-thalamus border. External validation analyzed show that effective stimulation engages a brain network overlapping with disrupted patterns of brain activity observed in two independent cohorts with impaired consciousness: one with arousal-impairing stroke lesions and the other with awareness-impairing seizures. Together, these findings advance the field by informing patient selection, refining stimulation targets, and identifying a brain network linked to recovery that may have broader therapeutic relevance across consciousness-impairing conditions.

There are no proven treatments for patients with chronic disorders of consciousness (DoC)[1,2]. DoC are caused by brain injuries including hypoxia, ischemia, trauma, and intracerebral hemorrhage, resulting in impairments in arousal or awareness that vary widely in severity and prognosis[3,4]. These patients commonly reside in long-term care facilities with little or no ability to engage with their environments—for months, years, even decades.

Neuromodulation has been explored as a potential therapy to restore consciousness in patients with DoC for over 50 years. Pioneering work by Hassler[5] and McLardy[6] in the 1960s was followed by larger case series of deep brain stimulation (DBS) in the 1990s[7,8] and later studies[9–19]. Various stimulation targets have shown some efficacy in uncontrolled trials, including: the intralaminar thalamus[7–9,12–14,16,17,19], brainstem[8,17], pallidum[5,11], and nucleus accumbens[15]. However, evidence from randomized controlled trials is lacking.

Recent advances in understanding the brain networks underlying DoC[20] have opened new avenues for diagnosis[1,2], treatment[21], and outcome prediction[4]. Regardless of etiology, DoC involve widespread suppression of excitatory neurotransmission[3], particularly within the anterior forebrain mesocircuit[20], which includes the frontal cortex, central thalamus, striatum, and brainstem.

Parallel advances have identified brain regions underlying transient or acute disruptions of consciousness in related conditions, such as generalized seizures[22] and post-stroke arousal impairments[23]. Whether these diverse conditions converge on a common, treatable brain network remains unknown.

Within the thalamus, the posterior intralaminar nuclei (centromedian [CM] and parafascicular [Pf] nuclei) are central components of the mesocircuit[20] and project directly to the striatum[24,25]. Based on these connections, the CM-Pf complex was targeted in a recent uncontrolled study of DBS for DoC[9,12], the largest of its kind, building on findings from previous, smaller studies[7,8,17,18]. While no consistent effects were seen at the group level, this study identified a subset of patients with dramatic improvements in consciousness in the first year following implantation—beyond what has been seen in natural history studies of chronic DoC[26,27].

Here, we analyzed patient-level data to test whether those who improved had specific clinical characteristics, including MRI measures of brain tissue integrity, that predicted treatment responsiveness. We also investigated whether they were stimulated in a specific thalamic subregion, white matter tract, or distributed functional brain network. Finally, we examined the external validity of this network by testing its involvement in two independent groups of patients with impairments of consciousness caused by stroke lesions or generalized seizures.

Results

Patient characteristics and clinical outcomes

The analysis cohort included 40 patients (29 males and 11 females; median age = 33 years, IQR = 19.5–52.5, range = 12–66) with DoC secondary to cardiac arrest or traumatic brain injury who met criteria for DBS based on previously described clinical, neurophysiologic, and neuroimaging evaluations[9,12]. Patients were assessed using the Coma Recovery Scale-Revised (CRS-R)[28] and classified as being in an unresponsive wakefulness syndrome (UWS), minimally conscious state (MCS), or conscious state[1]. Supplementary clinical measures included the Disability Rating Scale (DRS) and Coma/Near-Coma (C/NC) scale[29]. Detailed patient-level demographic and clinical characteristics are available in Supplementary Data 1. Example structural imaging findings illustrating the range of brain lesion patterns in the cohort are in Supplementary Fig. 1.

After a median of 6 months post-injury (IQR = 3.5–13, range = 2–137), patients underwent unilateral DBS targeting the left (n = 37) or right (n = 3) CM-Pf (Fig. 1). At 12 months post-DBS, 11 of 40 patients were classified as improved and 29 as non-improved. Improved patients were defined as those who transitioned from UWS to MCS or conscious, or from MCS to conscious, consistent with our previous work[9,12]. Across all patients, the median increase in total CRS-R scores was 2 (IQR = 2–7, range = 0–18; Fig. 1). Longitudinal CRS-R scores at additional timepoints (1, 3, 6, and 12 months post-implantation) are displayed in Supplementary Fig. 2. Three patients with UWS secondary to cardiac arrest died 3–6 months post-surgery due to cardiac complications, including recurrent arrest or progressive cardiopulmonary failure. For these patients, the outcome was defined based on the most recent follow-up prior to death. Sensitivity analyzed were conducted to test the robustness of findings using an alternative outcome definition (change in CRS-R score rather than binary classification). Additional sensitivity analyzed excluded patients with right-hemisphere DBS implants and those who died within 12 months post-implantation.

We first tested the hypothesis that clinical variables are associated with improvement (Table 1). Compared to non-improved patients, those who improved had less severe baseline impairments on the DRS and C/NC scales (p < 0.05, false discovery rate [FDR]-corrected) and, at an uncorrected threshold, were a median of 20 years younger at the time of injury. In contrast, the groups did not differ by sex, side of DBS, etiology of DoC, duration between initial injury and DBS, DBS lead model, or the programmed stimulation amplitude, frequency, or pulse width. The volume (mm³) of the modelled stimulation fields based on these settings also did not differ between groups (Supplementary Fig. 4; t(26) = 0.39, p = 0.7, Hedges' g = 0.15, 95% confidence interval (CI) = [−0.6, 0.9]), suggesting that outcomes may be more closely tied to the location of DBS rather than the parameters used.

Optimal brain tissue integrity

We next investigated whether DBS outcomes were associated with MRI measures of brain tissue integrity (Fig. 2). MRI scans were segmented into whole-brain compartments (gray matter, white matter, and cerebrospinal fluid) and regional subcortical volumes[30], then normalized by total intracranial volume and age-matched controls[31]. At an uncorrected significance threshold, patients who improved had greater preservation of whole-brain gray matter, as well as larger volumes of cerebellar gray matter and the dominant striatal targets of the CM-Pf, including the putamen and caudate. The groups did not differ in the volume of the pallidum, thalamus, brainstem, or ventral diencephalon (the region immediately inferior to the thalamus containing the hypothalamus and surrounding structures).

To explore whether a combination of volumetric MRI features could better distinguish between patients who improved and those who did not, we conducted a follow-up machine learning analysis using all whole-brain and subcortical volumes shown in Fig. 2 as input features. This analysis was performed using the Classification Learner App in MATLAB software (version R2023b), which evaluates the performance of various classifier models, including decision trees, support vector machines, k-nearest neighbors, and ensemble methods. The best-performing model was an ensemble of RUSBoosted decision trees, which integrates random under-sampling with boosting to address class imbalance[32]. This model achieved an accuracy of 84.6% and an area under the curve of 0.95 using 10-fold cross-validation (Supplementary Fig. 5). These results suggest that multivariate patterns of brain volume may offer additional discriminative value for predicting DBS outcomes beyond individual regional differences alone.

Optimal stimulation site

Electrodes were localized using Lead-DBS software[33]. This revealed variability in electrode placement across patients (Fig. 1), suggesting outcomes may depend on stimulation of specific thalamic subregions. To test this, we calculated electric fields (E-fields) for each patient, estimating the spatial extent and magnitude of stimulation based on individual DBS parameters[33,34]. E-fields were modeled using a finite element method (FEM) implemented in the adapted FieldTrip/SimBio pipeline[34], which simulates the distribution of electric potential in brain tissue. The E-field refers to the voxel-wise magnitude of the resulting electric field vector, measured in V/mm[33,35]. To identify stimulation sites associated with therapeutic benefit (Fig. 3), we performed voxel-wise two-sample t-tests comparing E-field magnitudes between improved and non-improved groups. This analysis revealed a candidate "sweet spot", defined by the largest surviving voxel cluster at a threshold of p < 0.05 (uncorrected; no voxels survived FDR correction). This region was located in the inferior Pf and subparafascicular nucleus, bordering the midbrain, with MNI152 ICBM 2009b coordinates (mm) of [X = −6.9, Y = −20.1, Z = −3.1]. No regions showed greater E-field magnitude in the non-improved group. To test the reliability of this site, we performed k-fold (k = 10) cross-validation, which confirmed its robustness (t(26) = 2.05, p = 0.047, Hedges' g = 0.8, 95% CI = [0.04, 1.7]), supporting the candidate sweet spot's association with clinical improvement.
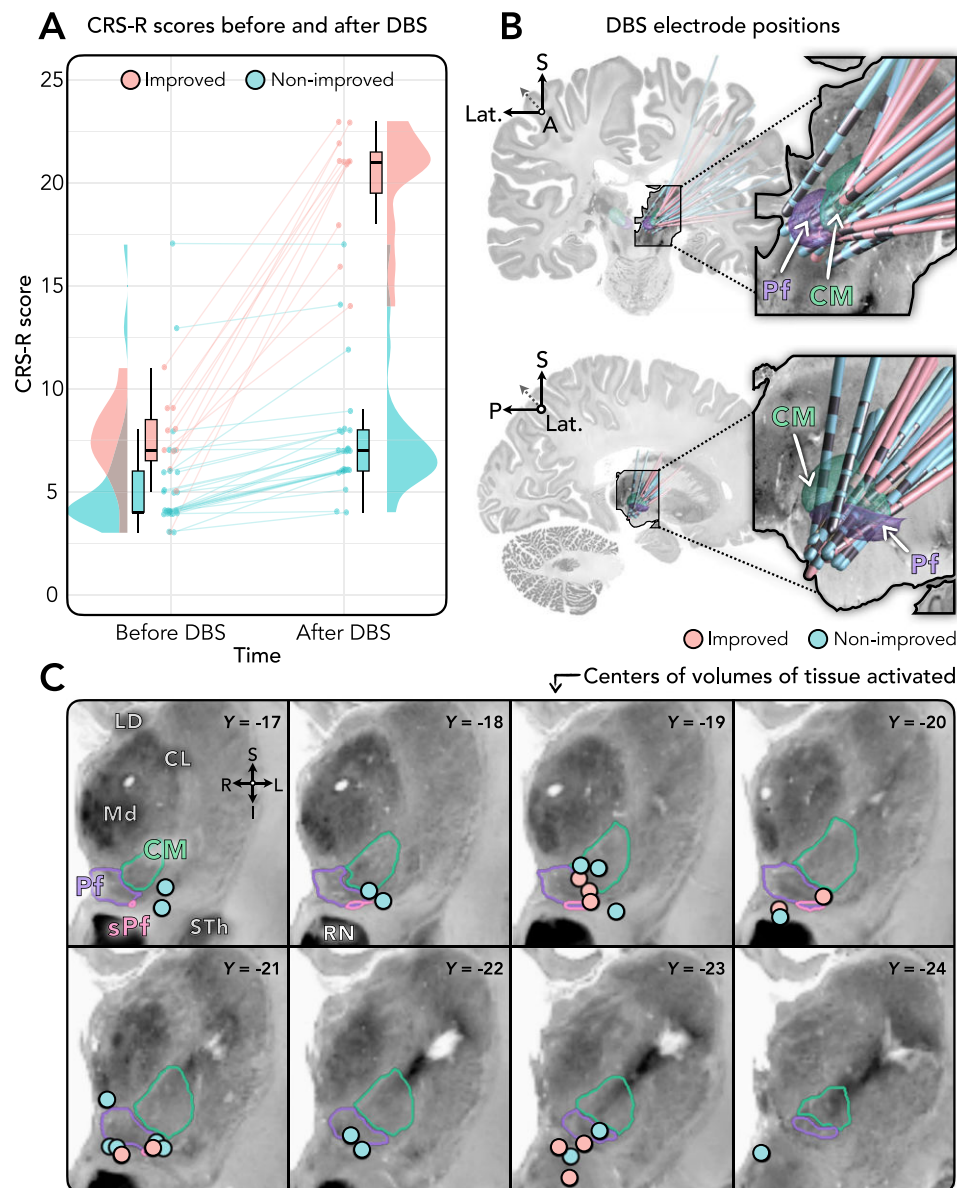
Fig. 1 | Clinical outcomes and DBS electrode localizations in improved and non-improved patient groups. A Raincloud plots[106] showing DoC severity before and 12 months after DBS, measured using the Coma Recovery Scale-Revised (CRS-R), where higher scores indicate better function. Patients were categorized as improved ($n = 11$; pink) or non-improved ($n = 29$; blue). Box plots show the median (thick line), interquartile range (IQR; 25th–75th percentile), and whiskers extending to 1.5× IQR. Individual patient scores are shown as jittered dots connected by lines; adjacent density plots show score distributions. Longitudinal scores at additional timepoints (1, 3, 6, and 12 months post-DBS) are shown in Supplementary Fig. 2. **B** Three-dimensional reconstructions of DBS electrodes. All leads were implanted unilaterally. Electrode positions are shown relative to the centromedian (CM) and parafascicular (Pf) nuclei, defined by the atlas of Krauth et al.[93] based on the histological work of Morel[107]. Supplementary Fig. 3 shows additional views of entry trajectories via the frontal lobe. Reconstructions were performed for patients with successful nonlinear image registrations to MNI space ($n = 10$ improved, $n = 18$ non-improved). **C** Coronal slices showing the centre of each patient's volume of tissue activated (i.e., the modelled electric field around stimulated contacts) overlaid on the BigBrain atlas[104] registered to MNI space[105]. Circles indicate locations from improved (pink; $n = 10$) and non-improved (blue; $n = 18$) patients. Y-coordinates reflect coronal slice position (mm) in MNI 152 ICBM 2009b nonlinear asymmetric template space. Individual patient coordinates are listed in Supplementary Data 1. Source data are provided as a Source Data file. Abbreviations: A, Anterior, CL, Central lateral nucleus, CM, Centromedian nucleus, CRS-R, Coma Recovery Scale−Revised, I, Inferior, L, Left, Lat., Lateral, LD, Lateral dorsal nucleus, Md, Mediodorsal nucleus, Pf, Parafascicular nucleus, R, Right, RN, Red nucleus, S, Superior, sPf, Subparafascicular nucleus, STh, Subthalamic nucleus.

Optimal structural connectivity

Having identified optimal DBS sites, we next hypothesized that improvement might be mediated by structural connections traversing areas of beneficial stimulation[33]. To test this, we calculated white matter streamlines using a normative diffusion MRI connectome acquired at an ultra-high resolution of $760\,\mu m$[36], as in our recent work[35,37]. Similar to the sweet spot analysis, which analyzed stimulation across voxels, we here compared E-field magnitudes across streamlines between improved and non-improved groups. This involved

conducting similar two-sample t-tests to identify streamlines more strongly engaged in the improved group, using an initial threshold of $p < 0.05$ (uncorrected; no streamlines survived FDR correction). The results were robust to k-fold ($k = 10$) cross-validation ($t(26) = 2.29$, $p = 0.03$, Hedges' $g = 0.9$, 95% CI = [0.18, 1.91]), supporting the reliability of these associations.

Improved patients showed greater involvement of a fiber bundle running along the border between the Pf/subparafascicular nucleus and midbrain, connecting brainstem nuclei with the hypothalamus.

Table 1 | Comparison of demographic and clinical variables between patients who improved (*n* = 11) and those who did not improve (*n* = 29) with DBS

	DoC improved (*n* = 11), median (IQR), or proportions	DoC non-improved (*n* = 29), median (IQR), or proportions	*p* value uncorrected (FDR-corrected), effect size (95% CI)
Age at injury (years)	19 (16–33)	39 (24.5–54)	*p* = 0.03 (0.14), Hedges' *g* = –0.78 (–1.63, –0.09)
Sex (Male:Female)	8:3	21:8	*p* = 1.0 (1.0), OR = 1.0 (0.21, 4.82)
Time from injury to DBS (months)	6 (3–12)	6 (3.5–14)	*p* = 0.67 (0.94), Hedges' *g* = –0.19 (–0.53, 0.56)
C/NC score before DBS#	2 (1–2)	3 (2–3.5)	*p* = 0.0009 (0.01), Hedges' *g* = –1.21 (–2.11, –0.58)
DRS score before DBS#	2.2 (1.8–2.6)	3.2 (2.6–3.5)	*p* = 0.003 (0.02), Hedges' *g* = –1.09 (–2.28, –0.47)
CRS–R score before DBS§	7 (6–9)	4 (4–6)	*p* = 0.06 (0.21), Hedges' *g* = 0.67 (0.06, 2.33)
DoC state prior to DBS (UWS:MCS)	8:3	26:3	*p* = 0.32 (0.75), OR = 0.31 (0.05, 1.84)
Implant side (Left:Right)	10:1	27:2	*p* = 1.0 (1.0), OR = 0.74 (0.06, 9.10)
Cause of injury (CA:TBI)	8:3	20:9	*p* = 1.0 (1.0), OR = 1.2 (0.26, 5.61)
DBS lead model (M3387:M3389:BSCI)	4:2:5	10:10:9	*p* = 0.6 (0.94)
Stimulation amplitude (V)†	3.25 (3–3.5)	3.25 (2.3–3.7)	*p* = 0.67 (0.94), Hedges' *g* = 0.2 (–0.33, 0.79)
Stimulation amplitude (mA)†	4.5 (4–5)	4.5 (4–5)	*p* = 0.75 (0.95), Hedges' *g* = 0.21 (–1.24, 1.05)
Stimulation frequency (Hz)	40 (25–40)	30 (25–30)	*p* = 0.13 (0.36), Hedges' *g* = 0.57 (–0.22, 1.6)
Stimulation pulse width (μs)	210 (210–210)	210 (180–210)	*p* = 0.38 (0.76), Hedges' *g* = 0.34 (–0.07, 0.8)

Continuous variables were compared using two-sided, non-parametric, permutation-based two-sample *t*-tests (10,000 permutations); categorical variables were compared using two-sided Fisher's exact tests. Results are reported as both uncorrected and false discovery rate (FDR)-corrected *p* values, with FDR correction applied across all 14 clinical and demographic variables tested.
BSCI Boston Scientific Vercise lead model, *CA* cardiac arrest, *CI* confidence interval, *C/NC* coma/near-coma, *M3387* medtronic lead model 3387, *M3389* medtronic lead model 3389; *MCS* minimally conscious state, *OR* Odds ratio, *DRS* disability rating scale, *TBI* traumatic brain injury, *UWS* unresponsive wakefulness syndrome.
#Note: a higher score on the C/NC scale and DRS indicates more severe impairment.
§Note: a higher score on the CRS-R scale indicates less severe impairment.
†Note: comparisons of stimulation amplitude were performed separately in patient sub-groups for whom amplitude was recorded as voltage (V; *n* = 6 improved vs. *n* = 20 non-improved) or milliamps (mA; *n* = 5 improved vs. *n* = 9 non-improved).

This pathway closely resembles portions of the VTT, a component of the ascending arousal network thought to sustain wakefulness in humans[38,39]. To assess similarity with the canonical VTT, we examined spatial overlap between the identified bundle and each of 16 nuclei previously defined as VTT contributors across the brainstem, thalamus, hypothalamus, and basal forebrain (see Table 1 in Edlow et al.[38]). Overlap was observed with 11 of 16 (69%) nuclei—specifically, the midbrain reticular formation (mRT), ventral tegmental area (VTA), periaqueductal gray (PAG), dorsal raphe (DR), parabrachial complex (PBC), locus coeruleus (LC), and laterodorsal tegmental nucleus (LDTg) of the brainstem, as well as the tuberomammillary nucleus (TMN), lateral hypothalamic area (LHA) and supramammillary nucleus (SUM) in the hypothalamus. Additional streamlines associated with improvement included pathways linking the cerebellar dentate nucleus, medial frontal cortex, and striatum (Fig. 4). No streamlines showed stronger involvement in non-improved patients.

Optimal functional connectivity
In the next analysis, we investigated blood-oxygen-level-dependent (BOLD) functional connectivity of DBS sites using a normative resting-state fMRI dataset acquired in 1000 healthy adults[40,41]. This involved overlaying each patient's E-fields on the normative fMRI data and calculating connectivity with all brain voxels. Connectivity strengths were then compared between improved and non-improved groups using voxel-wise two-sample *t*-tests, resulting in a map where positive *t*-scores indicate higher connectivity in the improved group (Fig. 5A).

The primary purpose of this analysis was to calculate a whole-brain, spatially continuous (i.e., unthresholded) map for subsequent comparison with external datasets of patients with stroke brain lesions and seizures associated with impaired consciousness (see below). However, to identify the cortical networks most implicated in improvement, we calculated the mean *t*-score within each of the seven canonical Yeo atlas networks[40]. Networks showing a positive mean *t*-score (i.e., more strongly associated with improvement) were, in descending order, the visual, dorsal attention, frontoparietal, and default-mode networks. In contrast, the somatomotor and ventral attention networks showed a negative mean *t*-score (i.e., more strongly associated with non-improvement). Applying a voxel-wise threshold of *p* < 0.05 (uncorrected), the improved group showed stronger connectivity with the hypothalamus, midbrain, pons, dorsal cerebellum, posterior hippocampus, and parieto-occipital fissure (Fig. 5A).

External validity: independent cohort analysis in patients with stroke
Our previous analyzed aimed to identify the brain network underlying favorable DBS outcomes. To assess the external validity of these findings, we tested—using an independent patient cohort—whether effective DBS for DoC modulates the same network disrupted by lesions causing acute arousal impairments. In other words, we hypothesized that the brain network where DBS improves consciousness (in our DoC cohort; Fig. 5A) overlaps with the network connected to lesions that disrupt consciousness (in an independent stroke cohort). Specifically, we included 45 previously described patients[23,42] who had
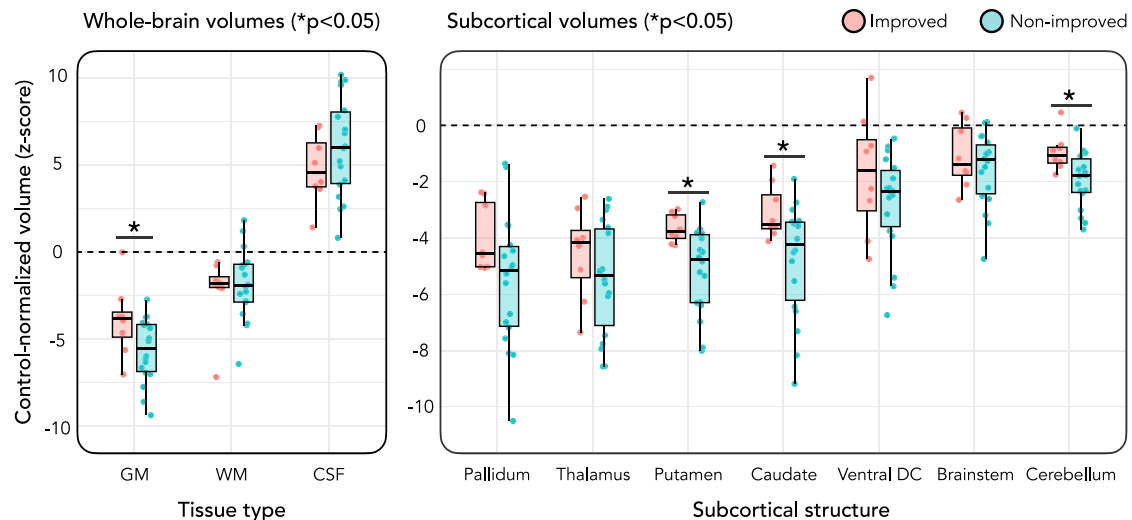
Fig. 2 | Comparison of MRI brain region volumes between improved and non-improved groups. Whole-brain tissue volumes (left panel: gray matter [GM], white matter [WM], and cerebrospinal fluid [CSF]) and regional subcortical gray matter volumes (right panel) are shown for the improved (pink) and non-improved (blue) groups. The dashed horizontal line indicates the average value in age-matched controls from the Nathan Kline Institute-Rockland Sample[31]. Volumes are expressed as z-scores relative to the control mean. Analyses included patients with available T1-weighted MRI ($n = 8$ improved; $n = 18$ non-improved). Box plots show the median (thick line), interquartile range (IQR; 25th–75th percentile), and whiskers extending to 1.5× IQR. Individual patient values are overlaid as jittered dots.

Statistical comparisons between groups were performed using two-sided, non-parametric, permutation-based t-tests (10,000 permutations). Four regions showed significantly greater volume in the improved group compared to the non-improved group (*$p < 0.05$, uncorrected): GM: $t(24) = 2.14$, $p = 0.04$, Hedges' $g = 0.9$, 95% CI = [0.14, 1.8]; Putamen: $t(24) = 2.7$, $p = 0.01$, Hedges' $g = 1.1$, 95% CI = [0.6, 1.8]; Caudate: $t(24) = 2.3$, $p = 0.03$, Hedges' $g = 0.9$, 95% CI = [0.4, 1.5]; Cerebellum: $t(24) = 2.6$, $p = 0.01$, Hedges' $g = 1.1$, 95% CI = [0.5, 1.8]. Source data are provided as a Source Data file. CSF Cerebrospinal fluid, GM Gray matter, WM White matter, Ventral DC Ventral diencephalon.

stroke involving the thalamus or brainstem. These patients were ordinally ranked based on the severity of their arousal impairment using scores from 1 to 6, with lower scores indicating more severe impairment. For each patient, we examined the brain network connected to their lesion using the same normative fMRI dataset described earlier[40,41], producing 45 lesion connectivity maps, each linked to a patient's arousal score. We then calculated the spatial similarity (Pearson correlation) between each lesion connectivity map and our DBS improvement network, predicting that higher similarity would correlate with worse outcomes (i.e., lower arousal scores). Consistent with this, we found that lesions associated with worse arousal impairment were connected to the positive regions in our DBS improvement network (Spearman $rho = -0.5$, $p = 0.0007$; Fig. 5B).

External validity: independent cohort analysis in patients with epilepsy

In a final analysis, we tested whether effective DBS for DoC modulates the same network disrupted by absence seizures, which are brief lapses of awareness marked by generalized spike-wave discharges on scalp EEG[22]. We used findings from a previous study of 15 patients with absence epilepsy who underwent simultaneous EEG-fMRI[43–45], a technique that can measure whole-brain BOLD signal changes time-locked to epileptiform EEG events. This analysis produced a group-level brain map showing areas linked to absence seizure-related disruption of awareness (Fig. 5C). As in our earlier analysis of arousal-impairing stroke lesions, we aimed to compare this EEG-fMRI map with our DBS improvement network, hypothesizing that the brain network where DBS improves consciousness overlaps with the network where seizures disrupt it. Using spin-permutation testing[46], we found that areas of BOLD signal suppression during generalized spike-wave discharges overlapped the positive regions in our DBS improvement network (Spearman $rho = -0.43$, $p = 0.026$); this BOLD suppression is thought to contribute to the transient lapses of awareness during absence seizures[22,47] and is most prominent in areas of the default-mode network[43–45].

Subgroup analyzed

Although the improved and non-improved groups differed significantly with respect to the location of stimulation, we noted that a subset of non-improved patients had sweet spot scores comparable to those of improved patients. Specifically, five non-improved patients had sweet spot scores exceeding the median value in the improved group (Fig. 3A). To explore this further, we compared these five patients to the remaining non-improved patients with lower sweet spot scores. The five with higher scores tended to be older (median 52 vs. 34 years) and exhibited more severe whole-brain gray matter atrophy (median z = −7.4 vs. −6 relative to controls), although these differences were not statistically significant. These trends suggest that patient-specific factors—such as age or structural integrity—may modulate responsiveness to stimulation, even when targeting is optimal.

Sensitivity analyzed

We performed several sensitivity analyzed to examine the consistency of our findings across three alternative analysis designs: (i) using a continuous outcome measure based on change in total CRS-R score (instead of a binary improved/non-improved classification), (ii) excluding three patients who died within 12 months of implantation, and (iii) excluding three patients with right- (instead of left-) hemisphere DBS implants (Supplementary Methods 1, Supplementary Tables 1–4, and Supplementary Figs. 6–9). All sensitivity analyzed continued to demonstrate that improvement was associated with less severe baseline impairment (DRS and C/NC scores), younger age at injury, and larger volumes of the putamen and cerebellum ($p < 0.05$, uncorrected). Regarding optimal structural connectivity, the distributions of fiber tracts linked to DBS improvement were similar to that in the primary analysis; findings remained robust to k-fold cross-validation when using CRS-R scores (Pearson $r = 0.42$, $p = 0.028$), and when excluding patients with right-hemisphere implants ($t(23) = 2.29$, $p = 0.03$, Hedges' $g = 0.92$, 95% CI = [0.17, 2.1]), but did not when excluding patients who died ($t(24) = 1.18$, $p = 0.25$, Hedges' $g = 0.47$,
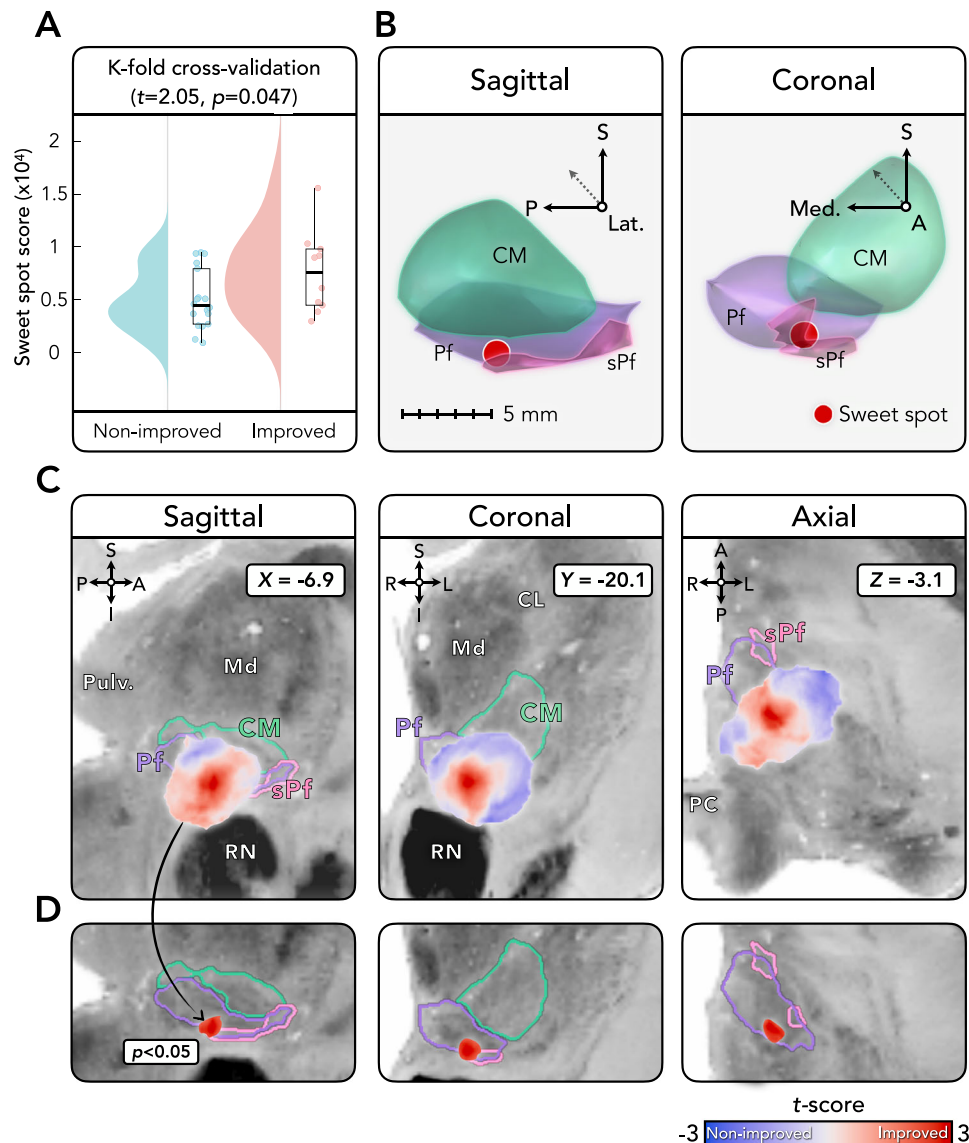
Fig. 3 | Anatomical localization and cross-validation of the optimal stimulation site. A K-fold cross-validation ($k = 10$) demonstrating that DBS E-field locations are significantly associated with clinical outcomes in left-out patients ($p = 0.047$; two-sided, non-parametric, permutation-based t-test, 10,000 permutations). Box plots show the median (thick line), interquartile range (IQR; 25th–75th percentile), and whiskers extending to 1.5× IQR. Individual patient values are overlaid as jittered dots. **B** Three-dimensional visualization of the stimulation sweet spot, defined as the center of gravity of the largest suprathreshold cluster ($p < 0.05$, uncorrected) identified via two-sided, voxel-wise, two-sample t-tests comparing E-field magnitudes between improved and non-improved groups. The sweet spot is displayed relative to the centromedian (CM), parafascicular (Pf), and subparafascicular (sPf) nuclei, as defined by the atlas of Krauth et al.[93] based on the histological work of Morel[107]. Analyses included patients with successful nonlinear image registration to MNI space ($n = 10$ improved, $n = 18$ non-improved). **C** Orthogonal slices showing the unthresholded t-score map. Positive values indicate voxels where E-field magnitude was higher in the improved group; negative values indicate higher E-field magnitude in the non-improved group. Slice coordinates (X, Y, Z) reflect mm positions in MNI152 ICBM 2009b nonlinear asymmetric template space. The unthresholded map is available in NIfTI format at: https://osf.io/bjah5. The map is displayed on the BigBrain atlas[104] registered to MNI space[105]. **D** Thresholded map ($p < 0.05$, uncorrected; two-sided, voxel-wise two-sample t-tests) highlighting the peak location associated with clinical improvement. Source data are provided as a Source Data file. A Anterior, CL Central lateral nucleus, I Inferior, L Left, Lat. Lateral, Md Mediodorsal nucleus, Med. Medial, P Posterior, PC Posterior commissure, Pulv Pulvinar nucleus, R Right, RN Red nucleus, S Superior.

95% CI = [−0.25, 1.36]). Finally, for optimal stimulation sites, the peak location associated with improvement ($p < 0.05$) remained within the inferior parafascicular nucleus abutting the midbrain and VTT in all sensitivity analyzed, less than 0.7 mm from the primary analysis peak in Fig. 3.

Discussion

Despite decades of research into DBS for DoC, critical questions have hindered prospective trials and broader clinical adoption: Which patients are ideal candidates? Where should stimulation be delivered for maximal effect? What brain networks mediate recovery, and do they generalize across conditions? Prior studies in individual cases or small cohorts have shown promising treatment effects but lacked the power to investigate biomarkers for patient selection or optimal targets. Here, we address these gaps by (i) identifying clinical and MRI features associated with improvement, (ii) delineating an optimal thalamic subregion and white matter pathway for stimulation, and (iii) linking effective DBS sites to a brain network that may hold therapeutic relevance across a broader range of consciousness-impairing conditions, including stroke and epilepsy.
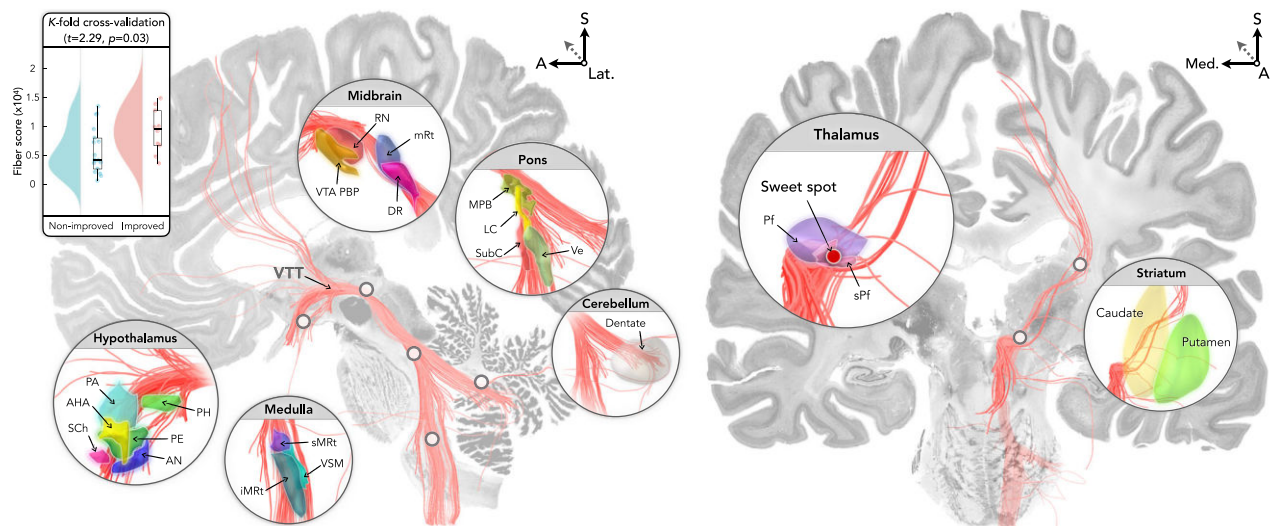
Fig. 4 | Anatomical localization and cross-validation of optimal structural connectivity. Box plots (top left) show results of k-fold (k = 10) cross-validation, demonstrating that structural connectivity is associated with clinical outcome in left-out patients (p = 0.03; two-sided, non-parametric, permutation-based t-test with 10,000 permutations). Box plots display the median (thick line), interquartile range (IQR; 25th–75th percentile), and whiskers extending to 1.5x IQR. Individual patient values are overlaid as jittered dots. Analyses included patients with successful nonlinear image registration to MNI space (n = 10 improved, n = 18 non-improved). Sagittal (left) and coronal (right) panels show white matter fiber tracts more strongly connected to the stimulation sites of improved versus non-improved patients (p < 0.05, uncorrected; two-sided, streamline-wise two-sample t-tests), including portions of the ventral tegmental tract (VTT)[38,39] that course along the midbrain-thalamus border to link the brainstem and hypothalamus. The previously identified stimulation sweet spot (Fig. 3) is indicated in the zoomed-in thalamic view. Results are displayed on the BigBrain atlas[104] registered to MNI space[105], with anatomical labels from the hypothalamus[95] (https://zenodo.org/records/3942115), brainstem (https://doi.org/10.25790/bml0cm.96), ascending arousal network[38] (https://doi.org/10.5061/dryad.zw3r228d2), thalamus[93] (https://zenodo.org/records/13918589), striatum[94], and cerebellum (https://www.diedrichsenlab.org/imaging/propatlas.htm). White matter fibre tract results are available as an NIfTI file at: https://osf.io/bjah5. Source data are provided as a Source Data file. A Anterior, AHA Anterior hypothalamic area, AN Arcuate nucleus, DR Dorsal raphe nucleus, iMRt Inferior medullary reticular formation, Lat. Lateral, LC Locus coeruleus, Med. Medial, MPB Medial parabrachial nucleus, mRt Mesencephalic reticular formation, PA Paraventricular nucleus, PE Periventricular nucleus, Pf Parafascicular nucleus, PH Posterior hypothalamus, RN Red nucleus, S Superior, SCh Suprachiasmatic nucleus, sMRt Superior medullary reticular formation, sPf Subparafascicular nucleus, SubC Subcoeruleus, Ve Vestibular nuclei complex, VSM Viscero-sensory-motor nuclei complex, VTA PBP Ventral tegmental area (parabrachial pigmented nucleus complex).

Improvement was more common in younger patients and those with intact gray matter volumes on structural MRI, particularly the striatum, the dominant projection of the CM-Pf. Like younger age, gray matter preservation may be essential for treatment effects of DBS to take hold, whether in the short term (i.e., acute functional changes requiring intact neuronal assemblies, such as synaptic transmission of stimulation) or longer term (i.e., chronic functional or structural neuroplastic changes)[48,49]. In keeping with this hypothesis, we previously found that effective CM-Pf DBS for DoC is associated with increases in gray matter volume lasting up to seven years post-DBS, including in the striatum[50].
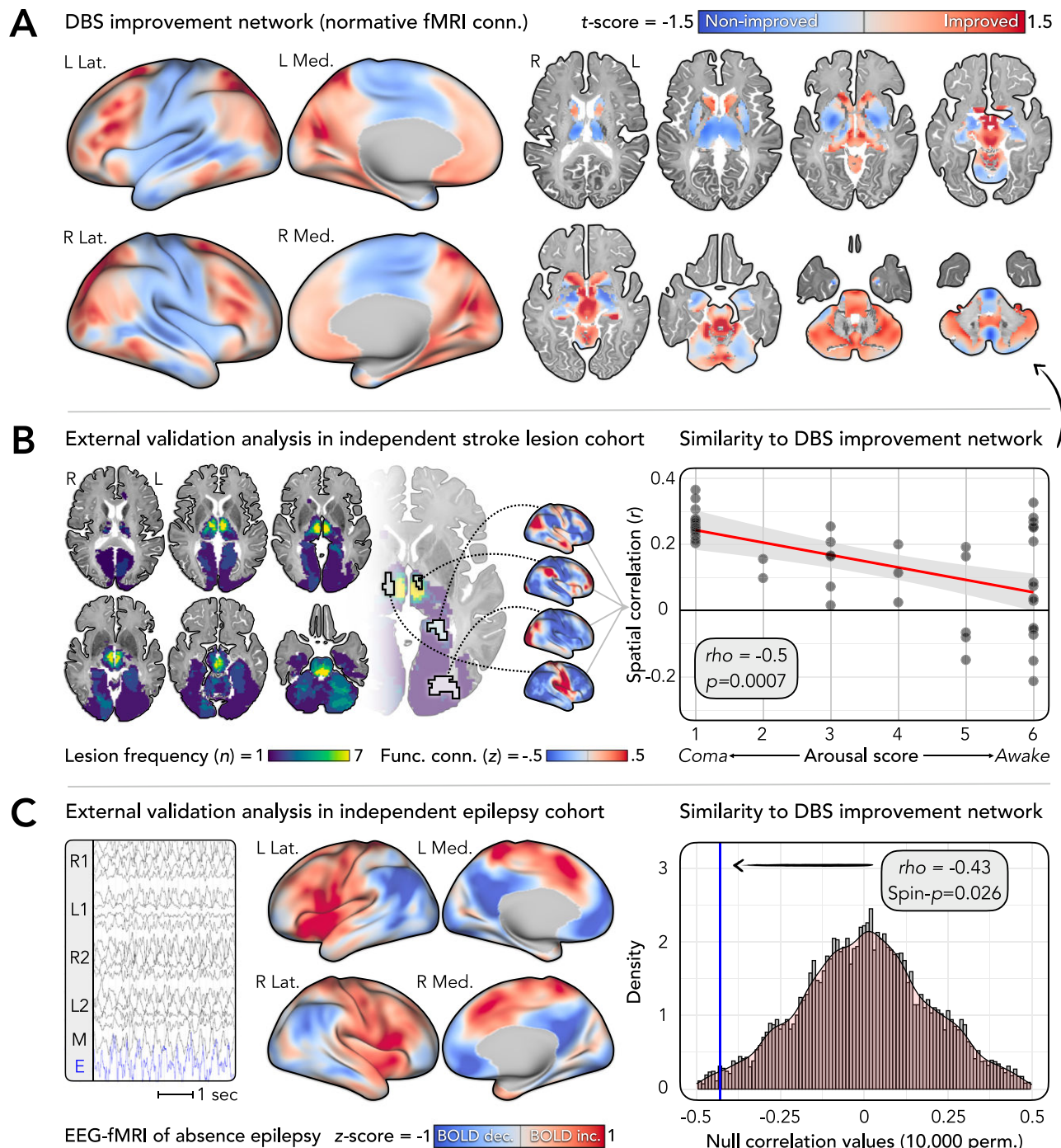
Preservation of the striatum and improved capacity for recovery are consistent with the mesocircuit model of DoC proposed by Schiff[20]. In this model, DoC emerge from a diffuse suppression of input from the cortex to striatal medium spiny neurons, leading to a loss of inhibitory projections to the globus pallidus and in turn a tonic inhibition of the thalamus, culminating in a breakdown of anterior forebrain arousal[20]. Increasing activity within this circuit, for example by DBS, is thus thought to restore consciousness. Preserved volume in improved patients suggests that the striatum may play a gating role[51] in restoring mesocircuit activity and thus could serve as a preoperative marker to identify optimal DBS candidates.

Despite targeting the CM-Pf region in all patients, there was natural variability in electrode placement and stimulation. Correlating this variability with outcomes, we found that improved patients had greater stimulation of the ventral and caudal Pf as well as the subparafascicular nucleus—a region abutting the ventral tegmental tract (VTT)[38,39] of the midbrain. Although the CM and Pf are often described as a unitary complex (CM-Pf), the two nuclei can be distinguished anatomically[52], functionally[53,54], and connectomically[24,25,55], which may confer differential stimulation effects. In primates, both nuclei are major sources of glutamatergic input to the striatum, but their projection profiles diverge: the CM targets striatal territories receiving input from sensorimotor cortex, particularly the caudal putamen, while the Pf projects to association and limbic territories, including the anterior putamen, caudate, and nucleus accumbens[24,25,55]. The caudal Pf—where stimulation appeared most effective—is known to project selectively to the caudate nucleus[56], suggesting that caudate-mediated circuits may play a particularly important role in recovery. The extrastriatal projections of the CM and Pf also differ, with the Pf sending more input to the hypothalamus, amygdala, and ventral tegmental area, and to prefrontal, anterior cingulate, and frontal eye field regions[24,25]. Among the posterior intralaminar nuclei, the subparafascicular nucleus has the densest descending projections to the brainstem, including the inferior olivary nucleus, peripeduncular area, reticular core, and raphe nuclei[25].

Our results complement recent studies of thalamic DBS for patients with TBI, which targeted the 'wing' of the central lateral (CL) nucleus[13,57], specifically the medial dorsal tegmental tract (DTTm). Like the CM-Pf, the CL is similarly thought to play a key role in arousal regulation via its striatal and frontal connections[58]. Experimental studies in non-human primates show that CL stimulation can facilitate task performance[59] and awaken animals from anesthesia[60]. Following an earlier case report[13], a recent randomized trial in six patients with TBI—none with DoC—found improvement in executive function after CL/DTTm DBS[57].

Direct comparisons of CL and CM-Pf stimulation are limited. One study found that stimulation of the CL, but not the CM-Pf, improved behavioral performance in macaques, with the authors suggesting that CL-specific improvements may stem from its selective projections to striatal medium spiny neurons and broad effects on the frontal lobe[59].

A DBS improvement network (normative fMRI conn.)

t-score = -1.5 [Non-improved — Improved] 1.5

L Lat. | L Med. | R | L

R Lat. | R Med.

B External validation analysis in independent stroke lesion cohort   Similarity to DBS improvement network

R | L

Lesion frequency (n) = 1 ▮ 7   Func. conn. (z) = -.5 ▮ .5

Spatial correlation (r)

rho = -0.5
p=0.0007

Coma ← Arousal score → Awake

C External validation analysis in independent epilepsy cohort   Similarity to DBS improvement network

R1 L1 R2 L2 M E

├─── 1 sec

L Lat. | L Med.

R Lat. | R Med.

EEG-fMRI of absence epilepsy z-score = -1 [BOLD dec. | BOLD inc.] 1

Density

rho = -0.43
Spin-p=0.026

Null correlation values (10,000 perm.)

However, another possibility is that therapeutic effects of these two targets converge not at the level of the CL and CM-Pf complex per se, but at the level of the CL-adjacent DTTm and the Pf-adjacent ventral tegmental tract, both of which originate from similar regions of the brainstem that project widely to the thalamus, hypothalamus, and forebrain[38,39]. Specifically, the two tracts emanate from a common point in the mesencephalic reticular formation[38,39], the same region first stimulated by Moruzzi and Magoun (1949) in their foundational work on the reticular activating system[61]. These results inspired the first clinical studies of brain stimulation to treat DoC[5,6].

This implies that the key determinant of DBS efficacy may not be stimulation of a single nucleus or sweet spot, but rather engagement of underlying arousal pathways that supply both regions[38,39]. Rather than viewing CL and CM-Pf stimulation as competing approaches, a more unified perspective suggests that both may be effective insofar as they modulate these shared pathways. This helps reconcile prior findings of similar behavioral benefits despite different targets[62] and provides a basis for optimizing stimulation by maximizing engagement of the circuit, rather than adhering strictly to one nucleus. Similarly, recent evidence from CM stimulation for generalized epilepsy suggests that stimulation of adjacent low activity regions—thought to reflect the internal medullary laminae surrounding the CM—can induce widespread cortical changes associated with seizure inhibition[63], supporting the idea that therapeutic effects may be mediated via stimulation of adjacent white matter circuitry rather than the nuclei themselves. The increasing practice of multi-target DBS[64], where several thalamic or other sites are stimulated simultaneously, may extend the feasibility of such circuit-targeted stimulation.

Fig. 5 | Optimal functional connectivity and alignment with brain networks disrupted in other consciousness-impairing conditions. A The DBS improvement network was derived by comparing the functional connectivity of stimulation sites between improved and non-improved groups using normative resting-state fMRI data[40,41]. The resulting map shows unthresholded *t*-scores, where positive values indicate regions with stronger connectivity in the improved group, and negative values indicate stronger connectivity in the non-improved group. Cortical surfaces are displayed on the fs_LR_32k template (https://balsa.wustl.edu/QXj2), and subcortical anatomy is shown using the BigBrain histological atlas[104] registered to MNI space[105]. The unthresholded map is available in GIfTI format at: https://osf.io/bjah5. Analyses included patients with successful nonlinear image registration to MNI space (*n* = 10 improved, *n* = 18 non-improved). **B** We assessed whether the DBS improvement network was associated with arousal outcomes in an independent cohort of 45 patients with arousal-impairing stroke lesions[23,42]. Axial slices show lesion frequency. For each lesion, a whole-brain connectivity map was computed, and its spatial similarity to the DBS improvement network was correlated with behavioral arousal ratings (6-point ordinal scale; lower scores = greater

impairment). The scatter plot shows a significant association (two-sided Spearman correlation), with a linear fit and 95% confidence interval overlaid. **C** We further compared the DBS improvement network to brain regions showing BOLD signal changes during generalized spike-wave discharges in 15 patients with absence epilepsy scanned using simultaneous EEG-fMRI[43-45]. An example EEG trace recorded inside the MRI scanner is shown using a longitudinal bipolar montage, with channels grouped by region: R1 = right lateral (Fp2-F8, F8-T4, T4-T6, T6-O2); L1 = left lateral (Fp1-F7, F7-T3, T3-T5, T5-O1); R2 = right parasagittal (Fp2-F4, F4-C4, C4-P4, P4-O2); L2 = left parasagittal (Fp1-F3, F3-C3, C3-P3, P3-O1); M = midline (Cz-Pz); E = electrocardiogram. EEG-fMRI results are displayed as z-score maps, where positive values indicate BOLD increases during discharges, and negative values indicate decreases. The histogram shows results from spin-permutation testing (10,000 spins)[46], revealing a significant negative correlation (two-sided Spearman correlation) between the EEG-fMRI map and the DBS improvement network. Source data are provided as a Source Data file. Conn. connectivity, EEG electroencephalogram, ECG electrocardiogram, Func. functional, L left, Lat. lateral, Med. medial, Perm. permutations, R right.

The pattern of optimal connectivity shows intriguing similarities to the neural circuitry underlying circadian regulation of arousal[65], which has been implicated in the pathophysiology and recovery of DoC[66,67]. Orexin-expressing neurons in the dorsomedial hypothalamus send dense projections to the locus coeruleus, the main site for norepinephrine synthesis, which has widespread excitatory effects[65]. Activity in the locus coeruleus shows circadian variation, promoting arousal during wakefulness and being inhibited during sleep, and is under direct control by projections from the hypothalamus[65]. Hypothalamic lesions disrupt this rhythm, causing somnolence, altered body temperature, and coma-like states[23,68]. Patients with DoC similarly show abnormal daily rhythms in EEG, temperature, and hormones[66,67]. The strength of circadian variation correlates with DoC severity, predicts recovery, and may even have therapeutic effects when exogenously entrained via, for instance, bright light stimulation[66,67]. These findings may relate to the integrity of neural circuits driving these circadian rhythms, consistent with our observation of enhanced connectivity from DBS sites to the hypothalamus and locus coeruleus in patients who showed improvement.

Our findings may aid with understanding pathophysiology, predicting outcomes, and developing new treatments, both for DoC and related conditions. Brain areas showing stronger connectivity with effective DBS sites overlapped with the networks underlying acute-onset lesions causing arousal impairments[23,42] and epileptiform events associated with transient lapses of awareness[43-45]. This suggests that effective stimulation targets for DoC might confer similar benefits across a broader spectrum of consciousness-impairing conditions. The findings may also aid with selecting cortical targets for non-invasive therapies like transcranial magnetic stimulation or transcranial direct current stimulation[21].

The choice of stimulation paradigm is an important consideration when comparing our findings to prior work. We used a medium stimulation frequency of 20–40 Hz, motivated by positive results in earlier studies[8,18], while others used higher frequencies of 100–185 Hz[10,13,57], likely having divergent effects[69]. The optimal paradigm for DoC, and whether it differs by target, brain state, or species, is uncertain. Several authors[59,60,70,71] have hypothesized that stimulation efficacy may partially depend on the intent of DBS—e.g., awakening from anesthesia or sleep versus enhancing arousal in an already conscious subject—as well as correspondence between the stimulation frequency and resonant (intrinsic) frequencies of the intended brain state. For example, 150–225 Hz stimulation of the CL facilitated task performance in awake macaques[71], echoing the high frequency of excitatory input required to trigger dendritic electrogenesis in neocortical neurons[71]. In contrast, another study found that CL stimulation at a lower (50 Hz), but not higher (200 Hz), frequency was effective at rousing macaques from propofol/isoflurane-induced anesthesia[60],

perhaps reflecting entrainment of central thalamic neurons that fire at similar frequencies (20–40 Hz) during wakeful states[72]. Conversely, low frequency (10 Hz) optogenetic stimulation of the central thalamus elicited spindle-like oscillations and behavioral arrest in rats[70], resembling patterns seen at the onset of sleep[73].

Hence, a possible reason for the efficacy of 20–40 Hz DBS seen here could be the alignment with thalamic oscillations during wakefulness—akin to its rousing effects in anesthetized subjects[60]. Consistent with this, Arnts et al. recently reported that 30–50 Hz DBS of the CM-Pf produced stronger treatment effects than 130 Hz stimulation in one patient with DoC[19] and another with akinetic mutism[74]. However, reports of contrary findings (e.g., restoration of consciousness during 130–180 Hz DBS in anesthetized macaques)[75,76] and potential interactions with other stimulation parameters (e.g., amplitude)[59,71,76] highlight the need for further research to elucidate optimal paradigms and mechanisms of action.

This study has limitations due to its clinical and retrospective nature. Patients had various DBS device models, with subtle differences in stimulation parameters, although not significantly associated with outcome. As in previous studies[10,11,15,18,57], the time between injury and DBS varied, and it is possible that natural recovery may have contributed to improvement in some patients; however, the lag time to DBS did not significantly differ between improved and non-improved groups, arguing against this as a major confound. Given the limited size of our cohort and the relatively small proportion of patients who showed improvement, several of our statistical analyzed were exploratory, with some results reaching significance only at the uncorrected level. In reporting these findings, we aimed to balance statistical rigor with the importance of preserving the clinically significant insights afforded by this rare dataset—insights that may guide future, more targeted analyzed. Nonetheless, replication in larger and prospectively acquired cohorts will be essential to confirm the robustness of these observations.

Patients showed structural brain abnormalities, including cortical injuries and diffuse atrophy, presenting challenges for accurate image registration and raising questions about using normative data[36,77] to assess connectivity in patient brains[33,78]. While normative connectivity provides a pragmatic framework for identifying candidate brain networks that could plausibly support therapeutic effects at the group level—particularly in heterogeneous populations lacking advanced imaging—it is important to recognize that patient-specific variability, including damage to the proposed pathways, may limit its relevance at the individual level. We mitigated this by excluding patients with severe abnormalities preventing accurate template alignment and assessed the predictive utility of our findings using cross-validation methods and examining external validity in patients with consciousness-impairing lesions[23,42] and seizures[43,44]. However,

replications using patient-specific and disease-matched connectomes will be important.

Methods

This study was conducted in accordance with the Declaration of Helsinki and approved by the institutional review board of Mass General Brigham, Boston. It involved retrospective analysis of a previous clinical study[9,12] conducted at Dubrava University Hospital, Croatia, which received ethical approval from the institutional review board of Dubrava University Hospital and the School of Medicine at the University of Zagreb. Informed consent was obtained from patients' families or caregivers. External validation analyzed used previously published results from two sources: (i) a study of patients with epilepsy approved by the human research ethics committee at Austin Health, Melbourne, with written informed consent obtained[43–45]; and (ii) studies of patients with stroke approved by the institutional review boards of the University of Iowa[23] and Mass General Brigham[42], which were exempted from obtaining informed consent based on secondary use of research data.

Methods overview: a pragmatic analysis approach

The neuroimaging and DBS outcome data described here present valuable opportunities to address key scientific and clinical questions in the treatment of DoC. However, this patient population presents unique challenges, including abnormal neuroanatomy[1–3] and low DBS response rates (~30% in previous studies[9,12,18]), making some conventional analytic approaches unsuited to such a rare and complex group. Given these challenges, we made several pragmatic decisions in our analysis and reporting approaches.

Accurate brain alignment to a common template is required for group-level analysis of optimal DBS locations and connectivity[33]. We excluded patients with severe brain abnormalities causing poor template alignment, as determined by two neuroimaging experts blinded to clinical outcomes. However, these patients were retained for analyzed not requiring template alignment, such as analysis of clinical variables associated with improvement. For clarity, the specific analyzed each patient's data contributed to are listed in Supplementary Data 1.

Patients did not undergo advanced MRI connectivity sequences, such as functional or diffusion MRI. For analysis of optimal connectivity profiles, we used normative connectivity data acquired in healthy participants, an approach we have previously used to generate robust predictive models of DBS outcome in Alzheimer's disease[35], epilepsy[79], Parkinson's disease[80], and more[33].

Patients and DBS surgery

The analysis cohort included 40 patients (29 males and 11 females; median age = 33 years, IQR = 19.5–52.5, range = 12–66). Sex was recorded based on caregiver report. A description of study procedures and outcomes from 32 of these patients has been previously published[9,12]. Patients were selected based on neurophysiologic, clinical, and neuroimaging evaluations[12]. Briefly, inclusion criteria included: (i) meeting clinical diagnostic criteria for UWS or MCS[81,82]; (ii) a minimum DoC diagnosis duration of 6 weeks (note that the median DoC duration was 6 months, and the lag time to DBS was not significantly different between improved and non-improved groups; Table 1); (iii) obtainable somatosensory evoked potentials (SSEP) via median nerve stimulation, with or without SSEPs from tibial nerve stimulation; (iv) periods of desynchronized scalp EEG activity observed during 12–24 h of monitoring; (v) sufficient hemodynamic and respiratory stability to undergo study procedures; and (vi) absence of significant lesions (e.g., hemorrhages or infarctions) in the brainstem, diencephalon, or basal ganglia[12]. This criterion was based on the hypothesis that recovery potential depends on the integrity of subcortical nuclei and their interactions with cortical networks[3]. For examples of patients who met and did not meet this criterion, see Fig. 1 in Chudy et al.[12]. Example structural imaging

findings illustrating the range of brain lesion patterns in included patients are shown in Supplementary Fig. 1.

The DBS procedure involved unilateral implantation of the CM-Pf. The rationale for unilateral, as opposed to bilateral, implantations was based on experience in prior studies[8,18], and to reduce surgical risk[8,18]. Most cases (37/40 patients) were implanted on the left (typically dominant) hemisphere, also motivated by experience in earlier studies[8,18]. The remaining 3/40 were implanted on the right due to left-sided injuries or anatomical variations that made the right thalamus a more feasible target. For group-level analyzed, we flipped these right DBS leads to the left hemisphere by mirroring patients' MRI/CT scans across the x-axis as a first step, prior to further image processing steps[33]. Sensitivity analyzed examined the consistency of our results when excluding these right-hemisphere patients.

Due to changes in market availability and hospital procurement policies over the study period, DBS device models varied and included Medtronic lead models 3387 or 3389, as well as Boston Scientific Vercise leads. Model type was not significantly associated with outcome (Table 1). Surgical target coordinates were defined on preoperative CT using the Schaltenbrand-Bailey[83] atlas: 4.5 mm anterior to the posterior commissure, 1 mm inferior to the inter-commissural line, and 4 mm lateral to the third ventricular wall. The inferior coordinate was chosen with the goal of placing the most distal DBS contact near the inferior border of the CM-Pf. The lateral coordinate was defined with respect to the third ventricular wall (rather than the inter-commissural line) to account for widened ventricles due to brain atrophy typically seen in this patient group[9,84].

Three days post-surgery, DBS devices were programmed to deliver a stimulation paradigm optimized per patient to elicit the strongest arousal reaction, as previously described[9,12]. Briefly, this involved testing each electrode contact using a stimulation frequency of 20–40 Hz, pulse width of 120–330 μs, and amplitude of 2–4.5 V or 2.5–5.5 mA. An arousal reaction was defined as eye opening (if the patient's eyes were closed), accompanied by mydriasis and a change in facial expression, with or without head turning and elevated blood pressure and heart rate[9,12]. Stimulation parameters for each patient are listed in Supplementary Data 1. Stimulation was administered for 30 min every 2 h during the day and discontinued at night with the aim of promoting circadian (sleep–wake) cycles[8].

Clinical outcomes

Outcomes were tracked using the CRS-R[28]. Total scores range from 0 to 23, with higher scores indicating a greater level of consciousness across auditory, visual, motor, oromotor, communication, and arousal subscales[28]. Supplementary clinical measures included the DRS and C/NC scale[29]. Patients were classified as being in a UWS, MCS, or conscious state[1]. We defined improved patients as those who transitioned from UWS to MCS or conscious, or from MCS to conscious, within 12 months post-implantation. Non-improved patients were those who did not change states, as in our previous work[9,12]. Dichotomizing the cohort into improved and non-improved groups was intended to increase sensitivity to factors driving clinically significant improvements in consciousness[85]. However, we performed sensitivity analyzed using each patient's change in CRS-R score to test consistency across a finer-grained definition of improvement.

DBS electrode localization and stimulation-induced electric fields

DBS electrodes were reconstructed using Lead-DBS software (Fig. 1)[33]. Given the study's retrospective nature, the types of pre- and postoperative imaging data varied (MRI, CT, or both). Electrode localizations were therefore optimized for each patient, based on available data. When a T1-weighted MRI scan was available (28/40 patients), it was used as the reference image for nonlinear spatial warping to template space; in other cases, we used CT. MRI scans were acquired

on a 1.5 T Siemens Avanto or Aera scanner using a volumetric T1-weighted magnetization-prepared rapid acquisition gradient echo (MPRAGE) sequence with a voxel resolution ≤1 mm³. CT scans were acquired using a Siemens scanner with slice thickness ≤0.5 mm.

We first linearly coregistered the post- to the preoperative image using Advanced Normalization Tools software[86], then calculated non-linear spatial warps to the Montreal Neurological Institute (MNI) 152 ICBM 2009b nonlinear asymmetric brain template. To accommodate the heterogeneous imaging modalities (MRI or CT) available for these non-linear warps, we used a recently developed deep learning-based tool, EasyReg[87], which can perform robust, modality-agnostic registrations[88], unlike classical techniques that rely on optimization of similarity metrics between images. As shown in Billot et al.[30], this strategy can cope with CT scans, despite their low soft-tissue contrast. This is because synthetic images with low contrast-to-noise ratios are regularly seen during model training[87]. To further optimize the performance of EasyReg for CT, we followed the approach of Billot et al.[30], and stretched the histogram of CT values in the soft-tissue interval (0 < HU < 80) using the piecewise linear tone-mapping function implemented in Lead-DBS software[33].

Accuracy of image registrations was reviewed by two authors (AELW and AH), blinded to clinical outcomes. Twelve patients were excluded from further analysis involving DBS localizations, primarily due to severe brain atrophy and/or grossly enlarged ventricles, resulting in poor template alignment. However, these patients were retained for other analyzed not requiring alignment to MNI space. Details of the specific patients included in each analysis are in Supplementary Data 1. Examples of appropriate and failed image registrations are shown in Supplementary Fig. 10.

DBS electrodes were localized using the PaCER[89] or TRAC/CORE[33] algorithm in Lead-DBS[33]. We then calculated electric fields (E-fields) for each patient's stimulation settings using the FEM within the adapted FieldTrip/SimBio pipeline (https://www.mrt.uni-jena.de/simbio/; http://fieldtriptoolbox.org/)[34]. E-fields represent the first derivative of the estimated voltage distribution applied to voxels in space; the field's magnitude is strongest near active electrode contacts and diminishes rapidly with distance[35]. The median E-field volume (thresholded at >200 V/m) was 284 mm³ (IQR = 240–348) in the improved group and 310 mm³ (IQR = 202–372) in the non-improved group, which was not a significant difference ($t(26) = 0.39$, $p = 0.7$, Hedges' $g = 0.15$, 95% CI = [−0.6, 0.9]). Examples of the smallest, median, and largest E-fields in each group are visualized in Supplementary Fig. 4.

Analysis of optimal brain tissue integrity

We assessed whether whole-brain and subcortical tissue volumes were associated with outcome, in patients with T1-weighted MRI scans available ($n = 8$ improved vs. $n = 18$ non-improved). Each patient's scan was segmented into whole-brain volumes of bilateral gray matter, white matter, and cerebrospinal fluid using SynthSeg software[30]. Additionally, we segmented regional subcortical volumes and carefully inspected the results for accuracy. To adjust for inter-patient variability in brain size, each segmented volume was normalized by the total intracranial volume. We also normalized by tissue volumes from age-matched samples of T1-weighted MRI scans from the Nathan Kline Institute-Rockland Sample (NKI-RS)[31]. This longitudinal, community-ascertained neuroimaging study includes >1500 individuals aged 6−85 years. For each DoC patient, we selected a subset of T1-weighted MRI scans from NKI-RS control participants (males and females) within a ±2-year age window. On average, we found 92 matching control participants per patient (range = 46−126). The NKI-RS scans were processed identically using SynthSeg[30], normalized by total intracranial volume, and used to convert each patient's whole-brain and subcortical volumes into z scores.

Analysis of optimal stimulation sites

To identify optimal stimulation sites, we compared E-fields between improved ($n = 10$) and non-improved ($n = 18$) groups[33]. As in prior studies[35,37], we focused on voxels covered by >25% of E-fields with a magnitude >200 V/m, a commonly assumed estimate of the voltage required to activate axons[35,90]. By default, Lead-DBS applies this threshold to the total cohort, which can, in extreme cases, lead to uneven group representation at certain voxels (e.g., 10 patients from one group and only 1 from the other). To ensure balanced group representation, we separately quantified E-field overlap across analyzed voxels for improved and non-improved groups (overlaps are visualized in Supplementary Fig. 4). Overlap ranged from 50 to 100% in the improved group and 44 to 100% in the non-improved group, indicating that retained voxels were consistently supported by data from both groups.

Next, we conducted a series of voxel-wise t-tests, resulting in a map of t-scores (t-map) where positive values indicate higher E-field magnitudes in the improved relative to non-improved patients. To identify a candidate site of optimal stimulation, the t-map was thresholded at $p < 0.05$ (uncorrected). While uncorrected voxel-wise thresholds have known limitations, their use is common in the literature on DBS sweet spots[35,79,91], and is motivated by two considerations: (i) the limited sample sizes in many exploratory DBS studies, and (ii) the high voxel resolution at which sweet spot analyzed are performed in Lead-DBS software (version 3.1; default resolution: 0.22 mm³). This resolution enhances anatomical specificity but substantially increases the number of voxel-wise comparisons. In our analysis, 26,892 voxels were tested at 0.22 mm³ resolution, corresponding to a total search volume of 5.9 cm³−approximately the size of one thalamus.

However, our primary inference was not based on this exploratory threshold alone. We subjected the identified cluster to k-fold cross-validation with $k = 10$, where k was the number of groups into which the dataset was randomly split[33,35]. A k of 10 was used to align with previous similar DBS studies[35,80]. We iteratively used k-1 folds for training and the remaining fold for testing. In each iteration, the t-map was recalculated, leaving out the E-fields of patients in the test fold. The clinical outcomes for the left-out patients were then estimated by calculating the peak value of a voxel-wise multiplication of their E-field distributions with the derived t-map. These estimates were then compared between the improved and non-improved patients using a non-parametric, permutation-based two-sample t test[92]. The intuitive interpretation of this analysis is that positive values in the t-map represent better stimulation locations. By testing whether E-fields from left-out patients more strongly overlapped with the positive sites in the t-map, we evaluated the robustness and potential predictive utility of our findings[33,35].

Analysis of optimal structural connectivity

To identify white matter tracts associated with improvement, we utilized the fiber filtering approach in Lead-DBS software with a normative structural connectome (Fig. 4)[33,35]. Given the potential importance of small and intricate connections within and around the thalamus and brainstem, we used a state-of-the-art, ultra-high resolution (760 μm) diffusion-weighted MRI dataset acquired across 18 h[36], as detailed in our recent work[35,37]. Like the analysis of optimal stimulation sites, which analyzed stimulations across voxels, here we examined stimulations across streamlines of the normative connectome using the same mass-univariate fashion. For each streamline and E-field pair, we recorded the peak magnitude that the streamline traversed. Then, we performed the same t-tests on the E-field magnitudes between improved ($n = 10$) and non-improved ($n = 18$) groups, yielding a t-score for each streamline, with positive t-scores indicating stronger exposure to E-fields in the improved group. To identify a candidate network of optimal structural connections, we again applied a threshold of $p < 0.05$ (uncorrected), then tested the robustness of this network using the same k-fold cross-validation ($k = 10$) procedure. Specifically, we iteratively assigned t-scores to streamlines, each time leaving out E-fields of patients in the test fold. We then computed the peak overlap between the left-out E-fields and the t-weighted streamlines for

each patient, comparing the results between groups[33,35] using a non-parametric, permutation-based two-sample *t*-test[92]. To define sub-cortical nuclei traversed by the observed fiber tracts, we compared results to anatomical atlases of the brainstem (https://doi.org/10.25790/bml0cm.96), ascending arousal network[38] (https://doi.org/10.5061/dryad.zw3r228d2), thalamus[93] (https://zenodo.org/records/13918589), striatum[94], cerebellum (https://www.diedrichsenlab.org/imaging/propatlas.htm), hypothalamus[95] (https://zenodo.org/records/3942115), and basal forebrain[96].

Analysis of optimal functional connectivity

We investigated BOLD functional connectivity of DBS sites using a normative, sex-balanced sample of resting-state fMRI scans from 1000 healthy adults (500 males, 500 females) from the Brain Genomics Superstruct Project[40,41]. The fMRI data and preprocessing pipeline are publicly available[77]. For each patient's E-field location, we extracted the mean BOLD time-course (from the normative scans) using a weighted average across all voxels with E-field magnitudes >200 V/m, then measured connectivity with every brain voxel using Fisher's *r*-to-*z* transformed Pearson correlations. Connectivity strengths were then compared between improved and non-improved groups using voxel-wise *t*-tests in permutation analysis of linear models (PALM) software[97]. The result of this analysis was a spatially continuous (i.e., unthresholded) map of brain areas showing stronger functional coupling with DBS sites linked to improvement (positive *t*-scores) or non-improvement (negative *t*-scores).

Alignment with consciousness-impairing stroke lesion network

We hypothesized that the brain network underlying DBS improvement in DoC may overlap with pathological circuits underlying consciousness-impairing stroke lesions. In other words, we reasoned that the network where stimulation improves consciousness may reflect the network where lesions disrupt it. To test this, we studied a group of 45 patients—unrelated to those who underwent DBS in the current study—who had acute-onset lesions in the thalamus or brainstem due to stroke (mean age ± 1 standard deviation = 58 ± 15 years; 31 males and 14 females; sex was recorded based on caregiver report). The patients were obtained from two sources: one study of patients with lesion-induced coma[42], and another of patients with variable outcomes ranging from coma to no impairment (i.e., awake)[23]. In the latter study, patients were ordinally ranked using scores from 1 to 6[23], based on clinical definitions of Plum and Posner[98], with lower scores indicating more severe impairment (coma = 1; stupor = 2; obtunded = 3; somnolent = 4; lethargic = 5; awake = 6). We combined the two datasets by assigning all coma patients a score of 1 while retaining the original rankings from the second study for patients with outcomes less severe than coma (i.e., scores from 2 to 6). Using the same normative fMRI dataset[40,41,77] described earlier, we used binary lesion masks as seeds to calculate functional connectivity with all brain voxels to create a lesion connectivity map for each patient. We then calculated a similarity score between each lesion connectivity map and our DBS improvement network (Fig. 5A) using spatial (Pearson) correlations. Finally, we tested whether higher similarity to our DBS improvement network was associated with more severe stroke outcome (i.e., lower arousal scores) using a rank-based, non-parametric Spearman correlation (Fig. 5B).

Alignment with consciousness-impairing seizure network

In a final analysis, we explored whether effective DBS sites for DoC modulate the same network that is disrupted by absence seizures, which are brief lapses in awareness marked by generalized spike-wave discharges (GSW) on scalp EEG. We used findings from a previous study of 15 patients with absence epilepsy who underwent up to 60 min of EEG-fMRI (mean age ± 1 standard deviation = 10 ± 5 years; 11 females and 4 males; sex was self-reported)[43–45]. GSW timings were manually marked on the EEG and used as regressors in a whole-brain fMRI analysis to identify discharge-related BOLD signal changes. Event-related independent component analysis (eICA)[43,99] was employed to detect BOLD patterns deviating from the canonical hemodynamic response function, often observed with epileptiform events[100,101]. The eICA was performed on temporally concatenated fMRI data from all patients, covering a 32-second window before and after GSW onset[43,99]. Thirteen brain components significantly associated with GSW were identified (*F*-test; *p* < 0.05, Bonferroni-corrected), each represented by a spatial map (*z*-scores) and a BOLD time-course. Positive *z*-scores indicated regions with increased BOLD signal (activation) while negative *z*-scores indicated decreased signal (deactivation). We averaged all *z*-score maps together to create one map representing overall patterns of activation/deactivation (Fig. 5C). Finally, both this map and the DBS improvement network were warped to FreeSurfer's fsaverage5 template[102]. Spatial similarity was then measured using a Spearman correlation, with statistical significance assessed via spin-permutation testing (10,000 spins)[46].

Statistical analyzed

Analyses were performed using MATLAB version R2023b. For comparison of clinical variables, MRI tissue volumes, sweet spot overlap, and optimal structural connectivity between improved and non-improved groups, we used two-sided, non-parametric, permutation-based *t*-tests (10,000 permutations; https://github.com/mickcrosse/PERMUTOOLS)[92] for continuous variables and Fisher's exact tests for between-group comparisons of categorical variables (https://www.mathworks.com/help/stats/fishertest.html). Effect sizes (Hedges' *g*) and bootstrapped 95% confidence intervals were calculated using the booteffectsize function in PERMUTOOLS[92]. Significance was defined using an alpha of 0.05 (two-sided). For hypothesis tests involving multiple comparisons, we report both uncorrected and Benjamini-Hochberg[103] FDR-corrected *p* values.

Reporting summary

Further information on research design is available in the Nature Portfolio Reporting Summary linked to this article.

Data availability

The optimal stimulation site (sweet spot), structural connectivity, and functional connectivity results are available at: https://osf.io/bjah5. The results are also included as an atlas in the Lead-DBS software package (www.lead-dbs.org). Raw patient MRI/CT data are not publicly available due to ethical restrictions. However, anonymized patient-level information—including stimulation coordinates, stimulation settings, and DBS outcomes—is provided in Supplementary Data 1 to support transparency and enable reproducibility of key aspects of the analysis. For visualization, we used the BigBrain atlas[104], registered to MNI space[105], available at: https://osf.io/xkqb3. The normative diffusion-weighted MRI and resting-state fMRI datasets used in this study are publicly available at: https://datadryad.org/stash/dataset/doi:10.5061/dryad.nzs7h44q2 and https://dataverse.harvard.edu/dataset.xhtml?persistentId=doi:10.7910/DVN/25833. The T1-weighted MRI scans from age-matched controls used in our analysis of regional brain volumes were obtained from the Nathan Kline Institute—Rockland Sample (NKI-RS), which can be accessed at: https://fcon_1000.projects.nitrc.org/indi/enhanced/. Source data are provided with this paper.

Code availability

All analyzed were performed using open-access code and software. Code for preprocessing and connectivity analyzed is available in Lead-DBS software version 3.1 (https://github.com/netstim/leaddbs). Data visualization was performed using Lead-DBS version 3.1 (https://github.com/netstim/leaddbs) and Connectome Workbench version 1.5.0 (https://github.com/Washington-University/workbench). Software to perform segmentation of whole-brain and subcortical volumes

from T1-weighted MRI scans is available as part of the FreeSurfer suite at: https://surfer.nmr.mgh.harvard.edu/fswiki/SynthSeg.

References

1. Giacino, J. T. et al. Practice guideline update recommendations summary: Disorders of consciousness: Report of the Guideline Development, Dissemination, and Implementation Subcommittee of the American Academy of Neurology; the American Congress of Rehabilitation Medicine; and the National Institute on Disability, Independent Living, and Rehabilitation Research. *Neurology* **91**, 450–460 (2018).

2. Kondziella, D. et al. European Academy of Neurology guideline on the diagnosis of coma and other disorders of consciousness. *Eur. J. Neurol.* **27**, 741–756 (2020).

3. Edlow, B. L. et al. Recovery from disorders of consciousness: mechanisms, prognosis and emerging therapies. *Nat. Rev. Neurol.* **17**, 135–156 (2021).

4. Fischer, D. & Edlow, B. L. Coma prognostication after acute brain injury: a review. *JAMA Neurol.* **81**, 4 (2024).

5. Hassler, R. et al. EEG and clinical arousal induced by bilateral long-term stimulation of pallidal systems in traumatic vigil coma. *Electroencephalogr. Clin. Neurophysiol.* **27**, 689–690 (1969).

6. McLardy, T. et al. Attempted inset-electrodes-arousal from traumatic coma: neuropathological findings. *Trans. Am. Neurol. Assoc.* **93**, 25–30 (1968).

7. Cohadon, F. & Richer, E. Stimulation cérébrale profonde chez les patients en état végétatif post-traumatique: 25 observations. *Neuro-chirurgie* **39**, 281–292 (1993).

8. Tsubokawa, T. et al. Deep-brain stimulation in a persistent vegetative state: follow-up results and criteria for selection of candidates. *Brain Inj.* **4**, 315–327 (1990).

9. Chudy, D. et al. Deep brain stimulation for the early treatment of the minimally conscious state and vegetative state: experience in 14 patients. *J. Neurosurg.* **128**, 1189–1198 (2018).

10. Magrassi, L. et al. Results of a prospective study (CATS) on the effects of thalamic stimulation in minimally conscious and vegetative state patients. *J. Neurosurg.* **125**, 972–981 (2016).

11. Lemaire, J. J. et al. Deep brain stimulation in five patients with severe disorders of consciousness. *Ann. Clin. Transl. Neurol.* **5**, 1372–1384 (2018).

12. Chudy, D. et al. Deep brain stimulation in disorders of consciousness: 10 years of a single center experience. *Sci. Rep.* **13**, 19491 (2023).

13. Schiff, N. D. et al. Behavioural improvements with thalamic stimulation after severe traumatic brain injury. *Nature* **448**, 600–603 (2007).

14. Yang, Y. et al. Long-term functional outcomes improved with deep brain stimulation in patients with disorders of consciousness. *Stroke Vasc. Neurol.* **8**, 368–378 (2023).

15. Rezai, A. R. et al. Improved function after deep brain stimulation for chronic, severe traumatic brain injury. *Neurosurgery* **79**, 204–211 (2016).

16. Wojtecki, L. et al. Modulation of central thalamic oscillations during emotional-cognitive processing in chronic disorder of consciousness. *Cortex* **60**, 94–102 (2014).

17. Yamamoto, T. et al. DBS therapy for a persistent vegetative state: ten years follow-up results. *Acta Neurochir. Suppl.* **87**, 15–18 (2003).

18. Yamamoto, T. et al. Deep brain stimulation for the treatment of vegetative state. *Eur. J. Neurosci.* **32**, 1145–1151 (2010).

19. Arnts, H. et al. Clinical and neurophysiological effects of central thalamic deep brain stimulation in the minimally conscious state after severe brain injury. *Sci. Rep.* **12**, 12932 (2022).

20. Schiff, N. D. Recovery of consciousness after brain injury: a mesocircuit hypothesis. *Trends Neurosci.* **33**, 1–9 (2010).

21. Thibaut, A. et al. Therapeutic interventions in patients with prolonged disorders of consciousness. *Lancet Neurol.* **18**, 600–614 (2019).

22. Blumenfeld, H. Impaired consciousness in epilepsy. *Lancet Neurol.* **11**, 814–826 (2012).

23. Hindman, J. et al. Thalamic strokes that severely impair arousal extend into the brainstem. *Ann. Neurol.* **84**, 926–930 (2018).

24. Parent, M. & Parent, A. Single-axon tracing and three-dimensional reconstruction of centre median-parafascicular thalamic neurons in primates. *J. Comp. Neurol.* **481**, 127–144 (2005).

25. Sadikot, A. F. & Rymar, V. V. The primate centromedian-parafascicular complex: anatomical organization with a note on neuromodulation. *Brain Res. Bull.* **78**, 122–130 (2009).

26. Katz, D. I. et al. Natural history of recovery from brain injury after prolonged disorders of consciousness: outcome of patients admitted to inpatient rehabilitation with 1-4 year follow-up. *Prog. Brain Res.* **177**, 73–88 (2009).

27. Nakase-Richardson, R. et al. Longitudinal outcome of patients with disordered consciousness in the NIDRR TBI Model Systems Programs. *J. Neurotrauma* **29**, 59–65 (2012).

28. Giacino, J. T., Kalmar, K. & Whyte, J. The JFK coma recovery scale-revised: measurement characteristics and diagnostic utility. *Arch. Phys. Med. Rehabil.* **85**, 2020–2029 (2004).

29. Rappaport, M. The disability rating and coma/near-coma scales in evaluating severe head injury. *Neuropsychol. Rehabil.* **15**, 442–453 (2005).

30. Billot, B. et al. SynthSeg: Segmentation of brain MRI scans of any contrast and resolution without retraining. *Med. Image Anal.* **86**, 102789 (2023).

31. Nooner, K. B. et al. The NKI-rockland sample: a model for accelerating the pace of discovery science in psychiatry. *Front. Neurosci.* **6**, 152 (2012).

32. Seiffert, C. et al. RUSBoost: a hybrid approach to alleviating class imbalance. *IEEE Trans. Syst., man, Cybern. -Part A: Syst. Hum.* **40**, 185–197 (2009).

33. Neudorfer, C. et al. Lead-DBS v3.0: mapping deep brain stimulation effects to local anatomy and global networks. *Neuroimage* **268**, 119862 (2023).

34. Vorwerk, J. et al. The FieldTrip-SimBio pipeline for EEG forward solutions. *Biomed. Eng. Online* **17**, 37 (2018).

35. Rios, A. S. et al. Optimal deep brain stimulation sites and networks for stimulation of the fornix in Alzheimer's disease. *Nat. Commun.* **13**, 7707 (2022).

36. Wang, F. et al. In vivo human whole-brain connectom diffusion MRI dataset at 760 microm isotropic resolution. *Sci. Data* **8**, 122 (2021).

37. Hollunder, B. et al. Mapping dysfunctional circuits in the frontal cortex using deep brain stimulation. *Nat. Neurosci.* **27**, 573–586 (2024).

38. Edlow, B. L. et al. Multimodal MRI reveals brainstem connections that sustain wakefulness in human consciousness. *Sci. Transl. Med* **16**, eadj4303 (2024).

39. Edlow, B. L. et al. Neuroanatomic connectivity of the human ascending arousal system critical to consciousness and its disorders. *J. Neuropathol. Exp. Neurol.* **71**, 531–546 (2012).

40. Yeo, B. T. et al. The organization of the human cerebral cortex estimated by intrinsic functional connectivity. *J. Neurophysiol.* **106**, 1125–1165 (2011).

41. Holmes, A. J. et al. Brain Genomics Superstruct Project initial data release with structural, functional, and behavioral measures. *Sci. Data* **2**, 150031 (2015).

42. Fischer, D. B. et al. A human brain network derived from coma-causing brainstem lesions. *Neurology* **87**, 2427–2434 (2016).

43. Masterton, R. A. et al. Absence epilepsy subnetworks revealed by event-related independent components analysis of functional magnetic resonance imaging. *Epilepsia* **54**, 801–808 (2013).

44. Warren, A. E. L. et al. Neurostimulation for generalized epilepsy: should therapy be syndrome-specific? *Neurosurg. Clin. N. Am.* **35**, 27–48 (2024).

45. Carney, P. W. et al. The core network in absence epilepsy. Differences in cortical and thalamic BOLD response. *Neurology* **75**, 904–911 (2010).

46. Alexander-Bloch, A. F. et al. On testing for spatial correspondence between maps of human brain structure and function. *Neuroimage* **178**, 540–551 (2018).

47. Guo, J. N. et al. Impaired consciousness in patients with absence seizures investigated by functional MRI, EEG, and behavioural measures: a cross-sectional study. *Lancet Neurol.* **15**, 1336–1345 (2016).

48. Veerakumar, A. & Berton, O. Cellular mechanisms of deep brain stimulation: activity-dependent focal circuit reprogramming? *Curr. Opin. Behav. Sci.* **4**, 48–55 (2015).

49. Thibaut, A. et al. Clinical response to tDCS depends on residual brain metabolism and grey matter integrity in patients with minimally conscious state. *Brain Stimul.* **8**, 1116–1123 (2015).

50. Raguz, M. et al. Structural changes in brains of patients with disorders of consciousness treated with deep brain stimulation. *Sci. Rep.* **11**, 4401 (2021).

51. Schiff, N. D. & Plum, F. The role of arousal and "gating" systems in the neurology of impaired consciousness. *J. Clin. Neurophysiol.* **17**, 438–452 (2000).

52. Jones, E. G. Neuroanatomy: The Thalamus. Edward G. Jones. Plenum, New York (1985).

53. Kim, J. P. et al. Centromedian-parafascicular deep brain stimulation induces differential functional inhibition of the motor, associative, and limbic circuits in large animals. *Biol. Psychiatry* **74**, 917–926 (2013).

54. Matsumoto, N. et al. Neurons in the thalamic CM-Pf complex supply striatal neurons with information about behaviorally significant sensory events. *J. Neurophysiol.* **85**, 960–976 (2001).

55. Sidibe, M., Pare, J. F. & Smith, Y. Nigral and pallidal inputs to functionally segregated thalamostriatal neurons in the centromedian/parafascicular intralaminar nuclear complex in monkey. *J. Comp. Neurol.* **447**, 286–299 (2002).

56. Smith, Y. et al. The thalamostriatal system in normal and diseased states. *Front. Syst. Neurosci.* **8**, 5 (2014).

57. Schiff, N. D. et al. Thalamic deep brain stimulation in traumatic brain injury: a phase 1, randomized feasibility study. *Nat. Med.* **29**, 3162–3174 (2023).

58. Shah, S. A. & Schiff, N. D. Central thalamic deep brain stimulation for cognitive neuromodulation - a review of proposed mechanisms and investigational studies. *Eur. J. Neurosci.* **32**, 1135–1144 (2010).

59. Janson, A. P. et al. Selective activation of central thalamic fiber pathway facilitates behavioral performance in healthy non-human primates. *Sci. Rep.* **11**, 23054 (2021).

60. Redinbaugh, M. J. et al. Thalamus modulates consciousness via layer-specific control of cortex. *Neuron* **106**, 66–75 e12 (2020).

61. Moruzzi, G. & Magoun, H. W. Brain stem reticular formation and activation of the EEG. *Electroencephalogr. Clin. Neurophysiol.* **1**, 455–473 (1949).

62. Cao, T. et al. Clinical neuromodulatory effects of deep brain stimulation in disorder of consciousness: a literature review. *CNS Neurosci. Ther.* **30**, e14559 (2024).

63. Ho, J. C. et al. Refining centromedian nucleus stimulation for generalized epilepsy with targeting and mechanistic insights from intraoperative electrophysiology. *Nat. Commun.* **16**, 5272 (2025).

64. Yang, A. I. et al. Multitarget deep brain stimulation for epilepsy. *J. Neurosurg.* **140**, 210–217 (2024).

65. Aston-Jones, G. et al. A neural circuit for circadian regulation of arousal. *Nat. Neurosci.* **4**, 732–738 (2001).

66. Gobert, F. et al. Twenty-four-hour rhythmicities in disorders of consciousness are associated with a favourable outcome. *Commun. Biol.* **6**, 1213 (2023).

67. Blume, C. et al. Significance of circadian rhythms in severely brain-injured patients: a clue to consciousness? *Neurology* **88**, 1933–1941 (2017).

68. Ranson, S. W. Somnolence caused by hypothalamic lesions in the monkey. *Arch. Neurol. Psychiatry* **41**, 1–23 (1939).

69. Vitek, J. L. Mechanisms of deep brain stimulation: excitation or inhibition. *Mov. Disord.* **17**, S69–S72 (2002).

70. Liu, J. et al. Frequency-selective control of cortical and subcortical networks by central thalamus. *Elife* **4**, e09215 (2015).

71. Baker, J. L. et al. Robust modulation of arousal regulation, performance, and frontostriatal activity through central thalamic deep brain stimulation in healthy nonhuman primates. *J. Neurophysiol.* **116**, 2383–2404 (2016).

72. Glenn, L. L. & Steriade, M. Discharge rate and excitability of cortically projecting intralaminar thalamic neurons during waking and sleep states. *J. Neurosci.* **2**, 1387–1404 (1982).

73. Steriade, M., McCormick, D. A. & Sejnowski, T. J. Thalamocortical oscillations in the sleeping and aroused brain. *Science* **262**, 679–685 (1993).

74. Arnts, H. et al. Deep brain stimulation of the central thalamus restores arousal and motivation in a zolpidem-responsive patient with akinetic mutism after severe brain injury. *Sci. Rep.* **14**, 2950 (2024).

75. Bastos, A. M. et al. Neural effects of propofol-induced unconsciousness and its reversal using thalamic stimulation. *Elife* **10**, e60824 (2021).

76. Tasserie, J. et al. Deep brain stimulation of the thalamus restores signatures of consciousness in a nonhuman primate model. *Sci. Adv.* **8**, eabl5547 (2022).

77. Cohen, A. et al. GSP1000 preprocessed connectome, Harvard Dataverse, https://doi.org/10.7910/DVN/ILXIKS (2020).

78. Boes, A. D. et al. Network localization of neurological symptoms from focal brain lesions. *Brain* **138**, 3061–3075 (2015).

79. Warren, A. E. L. et al. The optimal target and connectivity for deep brain stimulation in Lennox-Gastaut syndrome. *Ann. Neurol.* **92**, 61–74 (2022).

80. Rajamani, N. et al. Deep brain stimulation of symptom-specific networks in Parkinson's disease. *Nat. Commun.* **15**, 4662 (2024).

81. Multi-Society Task Force on, P. V. S. Medical aspects of the persistent vegetative state (1). *N. Engl. J. Med.* **330**, 1499–1508 (1994).

82. Giacino, J. T. et al. The minimally conscious state: definition and diagnostic criteria. *Neurology* **58**, 349–353 (2002).

83. Schaltenbrand, G. & Wahren, W. Atlas for stereotaxy of the human brain. 2nd edn. (Stuttgart: Thieme, 1977).

84. Singh, H. et al. Optimizing indirect targeting of the centromedian nucleus for deep brain stimulation by incorporating third ventricular anatomy. *J. Neurosurg.* **142**, 299–310 (2024).

85. Monti, M. M. et al. What is a minimal clinically important difference for clinical trials in patients with disorders of consciousness? a novel probabilistic approach. *PLoS ONE* **18**, e0290290 (2023).

86. Avants, B. B. et al. A reproducible evaluation of ANTs similarity metric performance in brain image registration. *Neuroimage* **54**, 2033–2044 (2011).

87. Iglesias, J. E. A ready-to-use machine learning tool for symmetric multi-modality registration of brain MRI. *Sci. Rep.* **13**, 6657 (2023).

88. Hoffmann, M. et al. SynthMorph: learning contrast-invariant registration without acquired images. *IEEE Trans. Med. Imaging* **41**, 543–558 (2021).

89. Husch, A. et al. PaCER - A fully automated method for electrode trajectory and contact reconstruction in deep brain stimulation. *Neuroimage Clin.* **17**, 80–89 (2018).

90. Astrom, M. et al. Relationship between neural activation and electric field distribution during deep brain stimulation. *IEEE Trans. Biomed. Eng.* **62**, 664–672 (2015).

91. Meyer, G. M. et al. Deep brain stimulation for obsessive-compulsive disorder: optimal stimulation sites. *Biol. Psychiatry* **96**, 101–113 (2024).

92. Crosse, M. J., Foxe, J. J., Molholm, S. Permutools: a MATLAB package for multivariate permutation testing. *ArXiv* https://arxiv.org/abs/2401.09401 (2024).

93. Krauth, A. et al. A mean three-dimensional atlas of the human thalamus: generation from multiple histological data. *Neuroimage* **49**, 2053–2062 (2010).

94. Xiao, Y. et al. A dataset of multi-contrast population-averaged brain MRI atlases of a Parkinson's disease cohort. *Data Brief.* **12**, 370–379 (2017).

95. Neudorfer, C. et al. A high-resolution in vivo magnetic resonance imaging atlas of the human hypothalamic region. *Sci. Data* **7**, 305 (2020).

96. Ding, S. L. et al. Comprehensive cellular-resolution atlas of the adult human brain. *J. Comp. Neurol.* **524**, 3127–3481 (2016).

97. Winkler, A. M. et al. Permutation inference for the general linear model. *Neuroimage* **92**, 381–397 (2014).

98. Posner, J. B. Plum and Posner's diagnosis of stupor and coma. *Crit. Care Med.* **36**, 2492 (2008).

99. Masterton, R. A., Jackson, G. D. & Abbott, D. F. Mapping brain activity using event-related independent components analysis (eICA): specific advantages for EEG-fMRI. *Neuroimage* **70**, 164–174 (2013).

100. Josephs, O., Turner, R. & Friston, K. Event-related fMRI. *Hum. Brain Mapp.* **5**, 243–248 (1997).

101. Buckner, R. L. Event-related fMRI and the hemodynamic response. *Hum. Brain Mapp.* **6**, 373–377 (1998).

102. Fischl, B. et al. High-resolution intersubject averaging and a coordinate system for the cortical surface. *Hum. Brain Mapp.* **8**, 272–284 (1999).

103. Benjamini, Y. & Hochberg, Y. Controlling the false discovery rate: a practical and powerful approach to multiple testing. *J. R. Stat. Soc. Ser. B Methodol.* **57**, 289–300 (1995).

104. Amunts, K. et al. BigBrain: an ultrahigh-resolution 3D human brain model. *Science* **340**, 1472–1475 (2013).

105. Xiao, Y. et al. An accurate registration of the BigBrain dataset with the MNI PD25 and ICBM152 atlases. *Sci. Data* **6**, 210 (2019).

106. Allen, M. et al. Raincloud plots: a multi-platform tool for robust data visualization. *Wellcome Open Res.* **4**, 63 (2019).

107. Morel, A., Magnin, M. & Jeanmonod, D. Multiarchitectonic and stereotactic atlas of the human thalamus. *J. Comp. Neurol.* **387**, 588–630 (1997).

Acknowledgements

Author contributions

Competing interests

Additional information

[1]Department of Neurosurgery, Mass General Brigham, Harvard Medical School, Boston, MA, USA. [2]Center for Brain Circuit Therapeutics, Brigham and Women's Hospital, Harvard Medical School, Boston, MA, USA. [3]Department of Neurosurgery, Dubrava University Hospital, Zagreb, Croatia. [4]School of Medicine, Catholic University of Croatia, Zagreb, Croatia. [5]University of Würzburg, Faculty of Medicine, Wurzburg, Germany. [6]Athinoula A. Martinos Center for Biomedical Imaging, Department of Radiology, Massachusetts General Hospital, Harvard Medical School, Charlestown, MA, USA. [7]Center for Neuro-technology and Neurorecovery, Department of Neurology, Massachusetts General Hospital, Harvard Medical School, Boston, MA, USA. [8]Hawkes Institute, University College London, London, United Kingdom. [9]Computer Science and Artificial Intelligence Laboratory, Massachusetts Institute of Technology, Cambridge, MA, USA. [10]Eastern Health Clinical School, Monash University, Melbourne, VIC, Australia. [11]Florey Institute of Neuroscience and Mental Health, Heidelberg, VIC, Australia. [12]Perelman School of Medicine, University of Pennsylvania, Philadelphia, PA, USA. [13]Departments of Neurology, Pediatrics, and Psychiatry, Carver College of Medicine, University of Iowa, Iowa City, IA, USA. [14]Institute for Network Stimulation, Department of Stereotactic and Functional Neurosurgery, University Hospital Cologne, Cologne, Germany. [15]Department of Neurosurgery, Massachusetts General Hospital, Harvard Medical School, Boston, MA, USA. [16]Department of Surgery, School of Medicine, University of Zagreb, Zagreb, Croatia. [17]These authors jointly supervised this work: Darko Chudy, John D. Rolston. ✉e-mail: awarren15@bwh.harvard.edu; jrolston@bwh.harvard.edu